Supporting Information

Cucurbit[8]uril-mediated Pseudo[2,3]Rotaxanes

Guanglu Wu,[†] István Szabó,[§] Edina Rosta,[§] and Oren A. Scherman[*,†]

[†] Melville Laboratory for Polymer Synthesis, Department of Chemistry, University of Cambridge, Lensfield Road, Cambridge CB2 1EW, UK.

§Department of Chemistry, King's College London, 7 Trinity Street, London, SE1 1DB, UK.

[*] E-mail: oas23@cam.ac.uk

Table of Contents

SI-1 Materials and methods

Materials. All the materials as following were purchased from commercial suppliers and used without further purification: 2,6-dibromoanthracene (98%, TCI), 1,4-dibromonaphthalene (98%, Acros Organics), 2,7-dibromonaphthalene (99%, Sigma-Aldrich), 1,4-dibromobenzene (98%, Alfa Aesar), 4-pyridinylboronic acid (90%, Sigma-Aldrich), tetrakis(triphenylphosphine) palladium(0) (99%, Alfa Aesar), 1-chloro-2,4-dinitrobenzene (98%, Alfa Aesar), *p*-toluidine (99%, Sigma-Aldrich), aniline (99.5%, Sigma-Aldrich), 4-isopropylaniline (99%, Sigma-Aldrich), 4-tert-butylaniline (99%, Sigma-Aldrich), 1-adamantanamine hydrochloride (97%, Sigma-Aldrich), 2,2-Dimethyl-2-silapentane-5-sulfonate sodium salt (97%, Sigma-Aldrich). All solvents and reagents were purchased from Sigma-Aldrich (UK) or Fisher Scientific and used as received. Cucurbit[8]uril (CB[8]) and CB[7] were synthesized and purified according to a published procedure[1]. Milli-Q water (18.2 MΩ·cm) was used for preparation of all non-deuterated aqueous solutions.

High Pressure Liquid Chromatography (HPLC). HPLC was employed to purify and collect dicationic species by using a Phenomenex C18 Kinetic-Evo column with a 5 micron pore size, a 110 Å particle size and with the dimensions 150 x 21.2 mm. A gradient from 5% acetonitrile 95% water to 100% acetonitrile was run with 0.1% TFA.

Nuclear Magnetic Resonance Spectroscopy (NMR). ^{1}H NMR, ^{13}C NMR, COSY, DOSY, and NOESY spectra were acquired in heavy water (D_2O) at 298 K and recorded on a Bruker AVANCE 500 with TCI Cryoprobe system (500 MHz) being controlled by TopSpin2. NOESY experiments were carried out using a standard pulse sequence 'noesygpphpp' with 2 s relaxation delay and 1000 ms mixing time. The concentration of CB[8] or CB[7] deuterated aqueous solution was calibrated by the internal standard, DSS sodium salt.

Variable-Temperature ^{1}H NMR (VT-NMR). ^{1}H NMR spectra with variable temperature were recorded by a Bruker AVANCE 500 with TCI Cryoprobe system (500 MHz). The temperature of 500 MHz and 200 MHz spectrometers is calibrated by MeOD (D, 99.8 %).

Diffusion Ordered SpectroscopY (DOSY). The ^{1}H DOSY experiments were carried out using a modified version of the Bruker sequence ledbpgp2s involving, typically, 32 scans over 16 steps of gradient variation from 10% to 80% of the maximum gradient. Diffusion coefficients were evaluated in Dynamic Centre (a standard Bruker software) and determined by fitting the intensity decays according to the following equation:

$$I = I_o\, e^{[-D\gamma^2 g^2 \delta^2 (\Delta - \delta/3)]}$$

where I and I_o represent the signal intensities in the presence and absence of gradient pulses respectively, D is the diffusion coefficient, $\boldsymbol{\gamma}$ = 26753 rad/s/Gauss is the ^{1}H gyromagnetic ratio, $\delta = 2.4$ ms is duration of the gradient pulse, Δ = 100 ms is the total diffusion time and g is the applied gradient strength. Monte Carlo simulation method was used for the error estimation of fitting parameters with a confidence level of 95%.

UV/Vis Spectroscopy and Fluorescence Spectroscopy. UV/Vis and fluorescence spectra were recorded on a Varian Cary 400 UV/Vis spectrophotometer and Varian Cary Eclipse fluorescence spectrophotometer, respectively, using a Hellma 114F-QS cuvette with 10x4 mm path length at 298 K.

Isothermal Titration Calorimetry (ITC). ITC experiments were carried out on a Microcal ITC200 at 298.15 K in 10 mM sodium phosphate buffer (pH = 7.0). The concentration of CB[8] was calibrated by the titration with a standard solution of 1-adamantanamine. In order to avoid bias or potentially arbitrary offsets caused by manual adjustment of baseline, all raw data (thermograms) of ITC were integrated by NITPIC (v.1.2.2), fitted in Sedphat (v.15.2b), and visualized through GUSSI (v.1.2.1).[2]

SI-2 Synthesis and characterization

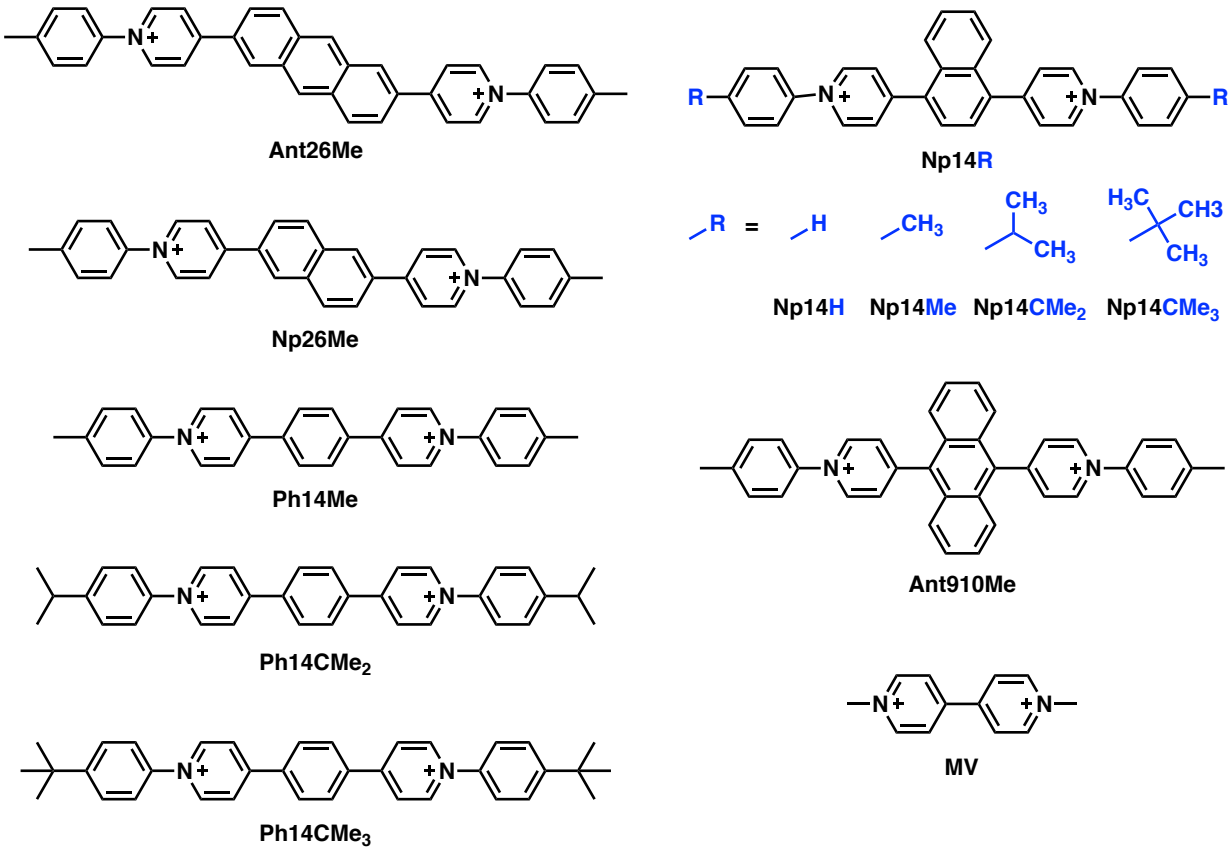

Scheme S1. Molecules related to this work (Counter anion is Cl^-).

As exemplified by **Ant26Me** in Scheme S2, a general synthesis of extended diarylviologen derivatives in this work starts with Suzuki-Miyaura cross-coupling[3] of two pyridin-4-yl groups onto the fluorophore core, followed by the transformation of the pryidin-4-yl groups into arylpyridinium salts through a Zincke reaction.[4]

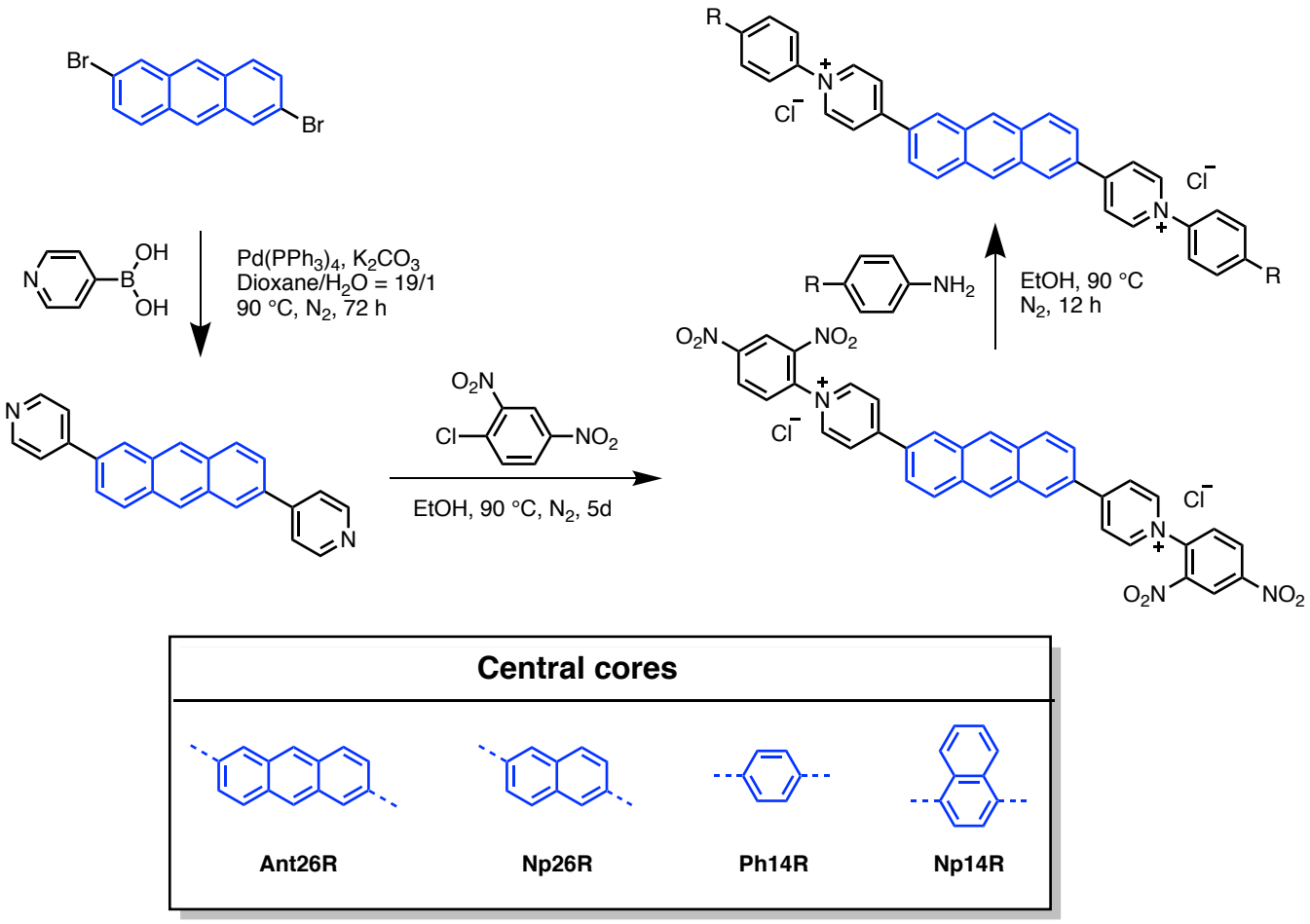

Scheme S2. Synthetic route of **Ant14Me** (when R = methyl).

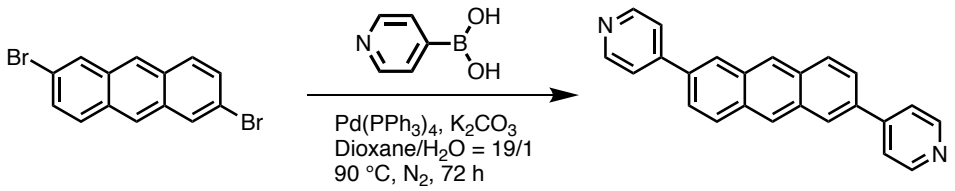

2,6-di(pyridin-4-yl)anthracene. $Pd(PPh_3)_4$ (192 mg, 0.17 mmol, 5 mol% of Br) was added into a mixture of 4-pyridinylboronic acid (500 mg, 3.66 mmol, 2.2 equiv.), 2,6-dibromoanthracene (582 mg, 1.66 mmol, 1 equiv.), and K_2CO_3 (1.6 g, 11.6 mmol, 7 equiv.) in the N_2-protected glove box. After three freeze-pump-thaw cycles, 16 mL of degassed dioxane/H_2O (19/1, v/v) were added into above mixture and stirred under nitrogen atmosphere for 72 h at 90 °C. After cooling to room temperature, the mixture was extracted with $CHCl_3$, washed with H_2O for three times, and dried over Na_2SO_4. The crude was concentrated and purified *via* a short silica gel column, firstly using ethyl acetate (EA) as eluent to remove fast-moving species followed by adding aqueous ammonia (35%) into the EA eluent (0.5% v/v) to collect the fluorescent spot. A yellow solid of 335 mg was obtained in 55% yield. ^{1}H NMR (500 MHz, $CDCl_3$) δ (ppm): 8.75 (d, J = 6.2 Hz, 2H), 8.57 (s, 2H), 8.32 (d, J = 1.7 Hz, 2H), 8.17 (d, J = 8.8 Hz, 2H), 7.79 (dd, J = 8.8, 1.8 Hz, 2H), 7.70 (d, J = 6.2 Hz, 2H). ^{13}C NMR (126 MHz, $CDCl_3$) δ (ppm): 150.59, 150.57, 148.13, 135.46, 132.20, 131.92, 129.60, 127.31, 126.92, 124.80, 121.89.

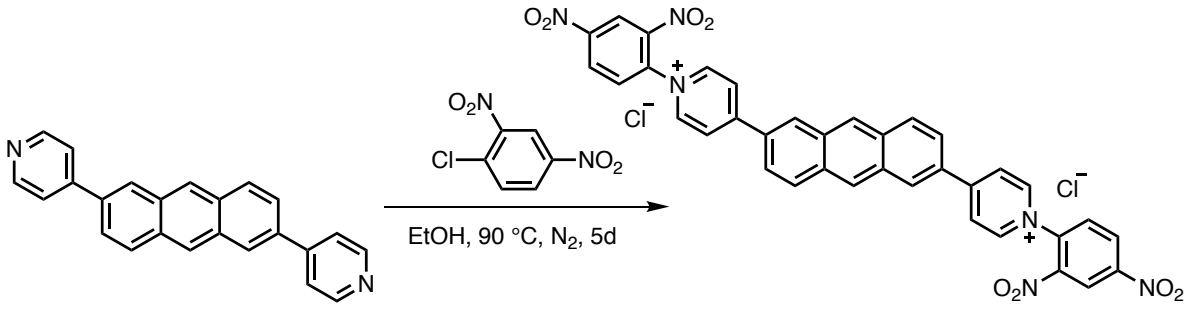

4,4'-(anthracene-2,6-diyl)bis(1-(2,4-dinitrophenyl)pyridin-1-ium) chloride (Ant26DNB). 1-Chloro-2,4-dinitrobenzene (0.77 g, 3.8 mmol, 12 equiv.) and 2,6-di(pyridin-4-yl)anthracene (110 mg, 0.33 mmol, 1 equiv.) were refluxed in ethanol (25 mL) at 90 °C for 5 days under nitrogen atmosphere (short reaction time will result in a large amount of mono-substituted product). After evaperating solvent under reduced pressure, the solid was re-dissolved in MeOH (3 mL) and was added dropwise into diethyl ether (120 mL) to precipitate products. Decantation of the supernatant after centrifuging by 8000 rpm for 10 mins at 4 °C afforded crude products (containing small amount of mono-substituted by-product) for further purification by HPLC. After drying by vacuum oven, the crude products were dissolved in ACN/H_2O mixture (40% v/v) and purified by a preparative reverse-phase HPLC using an eluent gradient of ACN/H_2O. The collected fraction was lyophilized to give 140 mg orange solid in 57% yield. ^{1}H NMR (500 MHz, Methanol-d_4) δ (ppm): 9.34 – 9.31 (m, 6H), 9.14 (d, J = 1.9 Hz, 2H), 8.98 (s, 2H), 8.96 (dd, J = 8.6, 2.5 Hz, 2H), 8.93 (d, J = 7.0 Hz, 4H), 8.48 (d, J = 8.9 Hz, 2H), 8.37 (d, J = 8.6 Hz, 2H), 8.26 (dd, J = 9.0, 2.0 Hz, 2H). ^{13}C NMR (126 MHz, Methanol-d_4) δ (ppm): 158.71, 149.77, 145.50, 143.44, 138.66, 132.99, 132.85, 131.63, 131.53, 131.26, 130.64, 129.72, 129.34, 124.62, 123.44, 121.85. LCMS: *m/z* $[M\text{-}2Cl]^{2+}$ calcd. for $C_{36}H_{22}N_6O_8^{2+}$: 333.1, found: 333.3.

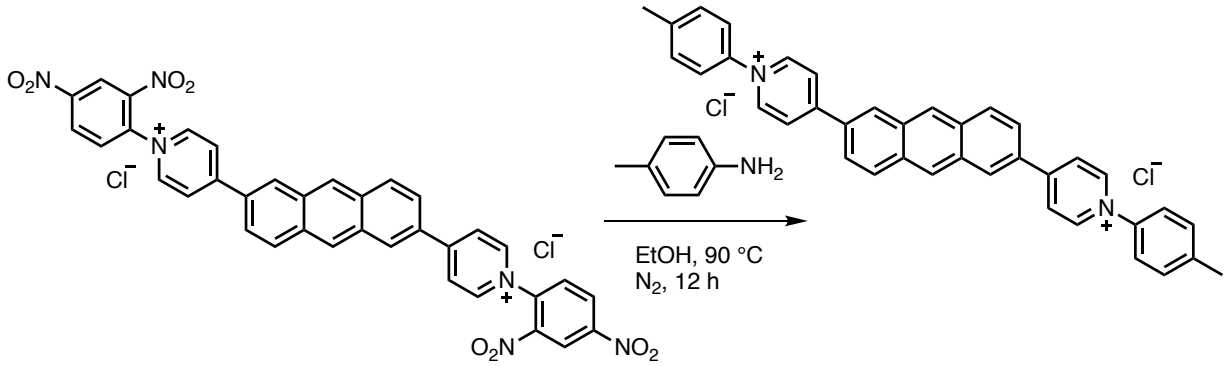

4,4'-(anthracene-2,6-diyl)bis(1-(p-tolyl)pyridin-1-ium) chloride (Ant26Me). *p*-Toluidine (35 mg, 0.33 mmol, 7 equiv.) and 4,4'-(anthracene-2,6-diyl)bis(1-(2,4-dinitrophenyl)pyridin-1-ium) chloride (35 mg, 0.05 mmol, 1 equiv.) were refluxed in ethanol (30 mL) at 90 °C for 12 h under nitrogen atmosphere. After removing solvent under reduced pressure, the solid was re-dissolved in MeOH (1 mL) and was added dropwise into diethyl ether (40 mL) to precipitate products. Decant the supernatant after centrifuging by 8000 rpm for 10 mins at 4 °C and repeat above MeOH-Ether step for another two times in order to wash off the excess of *p*-toluidine. Drying in vacuum oven gave 22 mg of orange solid in 79 % yield. ^{1}H NMR (500 MHz, Methanol-d_4) δ (ppm): 9.26 (d, J = 7.0 Hz, 4H), 9.03 (d, J = 1.9 Hz, 2H), 8.93 (s, 2H), 8.77 (d, J = 7.1 Hz, 4H), 8.44 (d, J = 8.9 Hz, 2H), 8.20 (dd, J = 9.0, 1.9 Hz, 2H), 7.77 (d, J = 8.5 Hz, 4H), 7.61 (d, J = 8.5 Hz, 4H), 2.54 (s, 6H). ^{13}C NMR (126 MHz, Methanol-d_4) δ (ppm): 157.90, 145.67, 143.76, 141.77, 134.22, 134.13, 133.19, 132.25, 132.00, 131.85, 130.33, 126.22, 125.04, 124.88, 21.19. LCMS: *m/z* [M-2Cl]$^{2+}$ calcd. for $C_{38}H_{30}N_2^{2+}$: 257.1, found: 257.4.

Products with different fluorophore cores and end groups were synthesized *via* the similar procedures as **Ant26Me**. **Np14DNB, Np14R**, **Ph14DNB,** and **Ph14Me** were obtained from our previous work.[5]

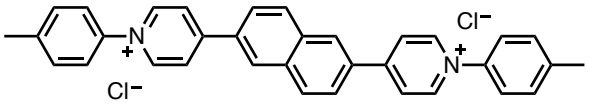

2,6-di(pyridin-4-yl)naphthalene. 250 mg (Yield: 55 %) ^{1}H NMR (500 MHz, $CDCl_3$) δ (ppm): 8.72 (d, J = 5.2 Hz, 4H), 8.16 (d, J = 1.8 Hz, 2H), 8.04 (d, J = 8.5 Hz, 2H), 7.81 (dd, J = 8.4, 1.7 Hz, 2H), 7.65 (d, J = 5.2 Hz, 4H).

4,4'-(naphthalene-2,6-diyl)bis(1-(2,4-dinitrophenyl)pyridin-1-ium) chloride (Np26DNB). 360 mg (Yield: 97 %) ^{1}H NMR (500 MHz, MeOD) δ (ppm): 9.37 (d, J = 7.0 Hz, 4H), 9.30 (d, J = 2.5 Hz, 2H), 8.96 (d, J = 2.5 Hz, 1H), 8.95 (d, J = 2.4 Hz, 3H), 8.92 (d, J = 7.0 Hz, 4H), 8.46 (d, J = 8.5 Hz, 2H), 8.40 (d, J = 8.7 Hz, 2H), 8.36 (dd, J = 8.7, 1.9 Hz, 2H). ^{13}C NMR (126 MHz, Methanol-d_4) δ (ppm): 159.92, 151.10, 147.08, 144.71, 140.05, 136.39, 134.83, 132.77, 132.69, 131.17, 131.12, 126.75, 126.36, 123.21. LCMS: *m/z* [M-2Cl]$^{2+}$ calcd. for $C_{32}H_{20}N_6O_8^{2+}$: 308.1, found: 308.3.

4,4'-(naphthalene-2,6-diyl)bis(1-(p-tolyl)pyridin-1-ium) chloride (Np26Me). 30 mg (Yield: 95%) ^{1}H NMR (500 MHz, D_2O) δ (ppm): δ 9.08 (d, J = 6.5 Hz, 4H), 8.68 (d, J = 1.7 Hz, 2H), 8.55 (d, J = 6.6 Hz,

4H), 8.35 (d, J = 8.7 Hz, 2H), 8.18 (d, J = 8.6 Hz, 2H), 7.67 (d, J = 8.2 Hz, 4H), 7.53 (d, J = 8.2 Hz, 4H), 2.47 (s, 6H). ^{13}C NMR (126 MHz, D_2O) δ (ppm): 155.52, 143.31, 142.56, 134.14, 132.92, 130.94, 130.87, 128.85, 125.39, 124.90, 124.76, 123.26, 20.20. LCMS: *m/z* $[M\text{-}2Cl]^{2+}$ calcd. for $C_{34}H_{28}N_2^{2+}$: 232.1, found: 232.8.

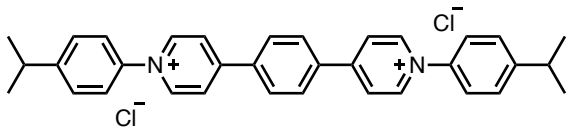

4,4'-(1,4-phenylene)bis(1-(4-isopropylphenyl)pyridin-1-ium) chloride (Ph14CMe$_2$). 10 mg (Yield: 95%) ^{1}H NMR (500 MHz, D_2O) δ (ppm): δ 9.14 (d, J = 6.9 Hz, 4H), 8.59 (d, J = 6.8 Hz, 4H), 8.29 (s, 4H), 7.74 (d, J = 8.6 Hz, 4H), 7.67 (d, J = 8.6 Hz, 4H), 3.12 (p, J = 6.9 Hz, 2H), 1.33 (d, J = 6.9 Hz, 12H). ^{13}C NMR (126 MHz, D_2O) δ (ppm): 155.56, 153.29, 144.06, 140.02, 137.00, 129.30, 128.53, 125.30, 123.70, 33.39, 22.95. LCMS: *m/z* $[M\text{-}2Cl]^{2+}$ calcd. for $C_{34}H_{34}N_2^{2+}$: 235.1, found: 235.5.

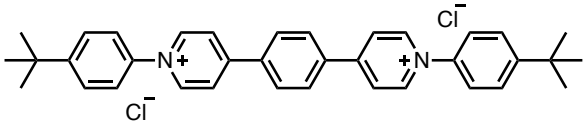

4,4'-(1,4-phenylene)bis(1-(4-(tert-butyl)phenyl)pyridin-1-ium) chloride (Ph14CMe$_3$). 9 mg (Yield: 94%) ^{1}H NMR (500 MHz, D_2O) δ (ppm): δ 9.15 (d, J = 6.8 Hz, 4H), 8.59 (d, J = 6.8 Hz, 4H), 8.30 (s, 4H), 7.84 (d, J = 8.8 Hz, 4H), 7.75 (d, J = 8.7 Hz, 4H), 1.41 (s, 18H). ^{13}C NMR (126 MHz, D_2O) δ (ppm): 155.66, 155.53, 144.07, 139.80, 137.04, 129.30, 127.58, 125.34, 123.41, 34.40, 30.29. LCMS: *m/z* $[M\text{-}2Cl]^{2+}$ calcd. for $C_{36}H_{38}N_2^{2+}$: 249.2, found: 249.6.

SI-3 Complexation of Ant26Me with CB[7] and CB[8]

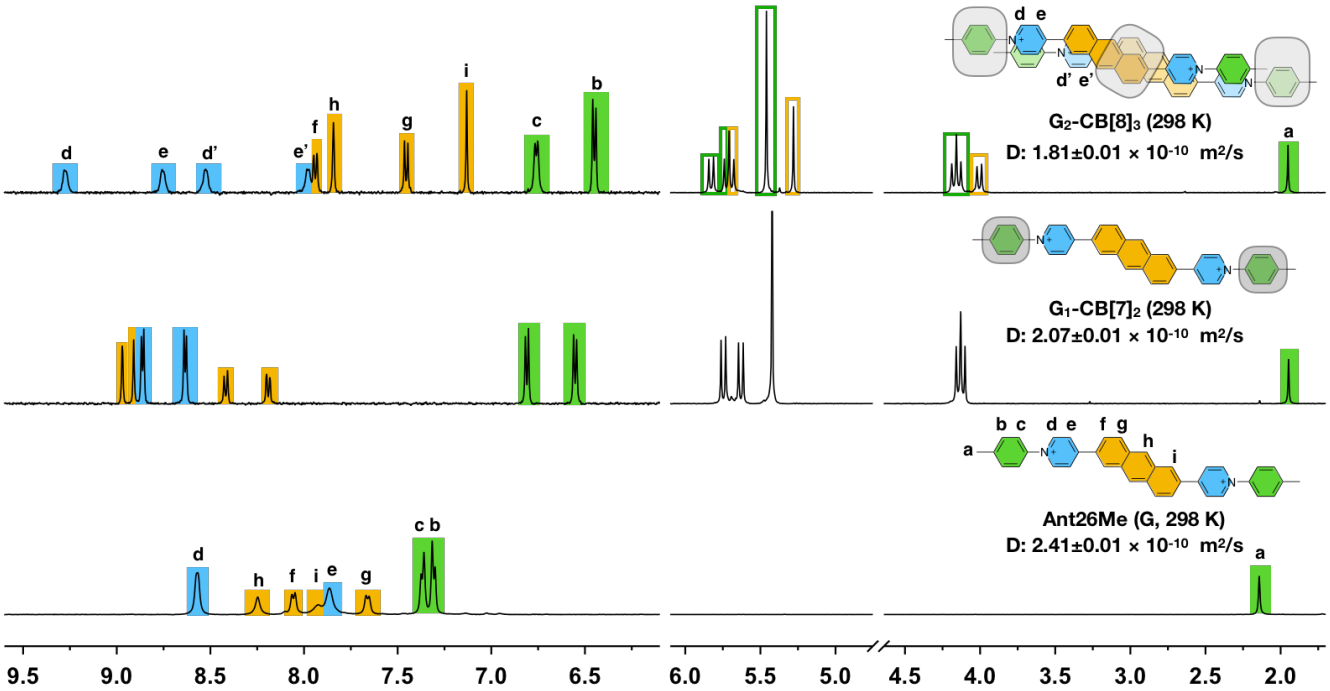

Figure S1. ^{1}H NMR spectra of **Ant26Me** (G), G_1-CB[7]$_2$, and G_2-CB[8]$_3$ complexes in D_2O at 298 K.

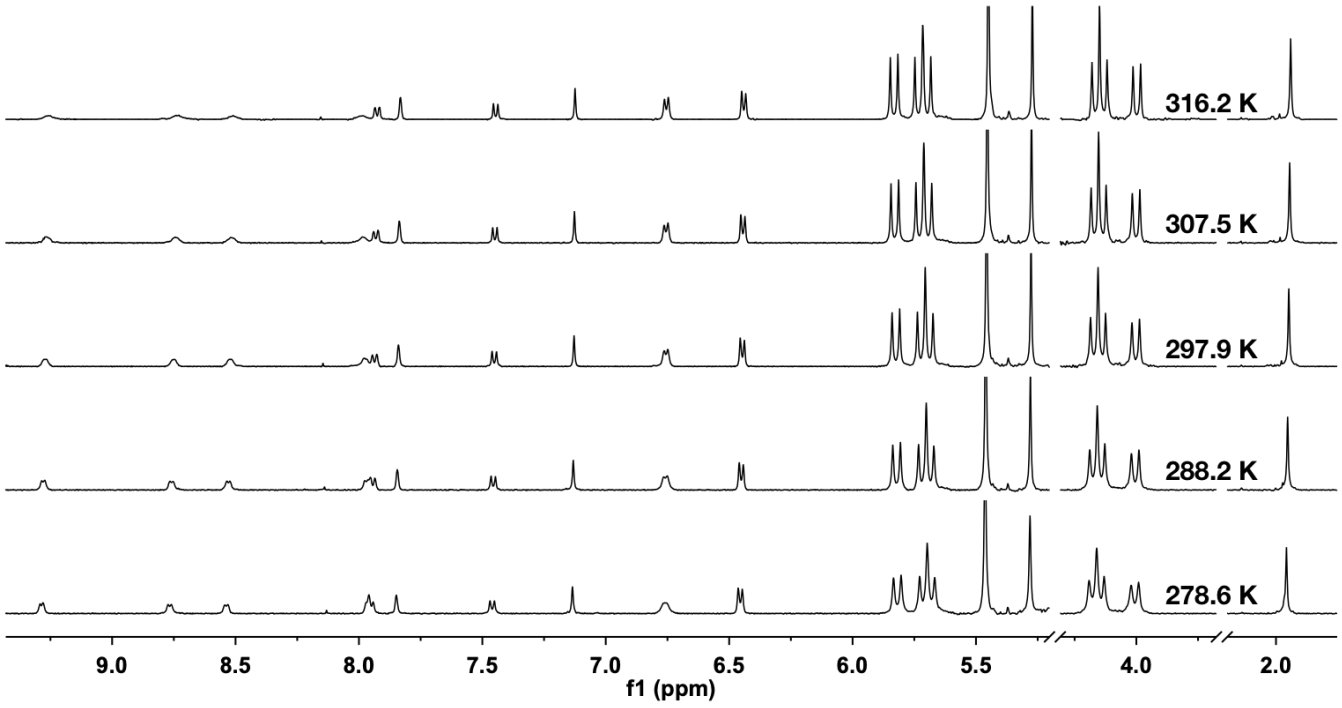

Figure S2. VT-NMR spectra of **Ant26Me$_2$**-CB[8]$_3$ D_2O solution (65 μM). Temperature was calibrated by MeOD (99.8% D).

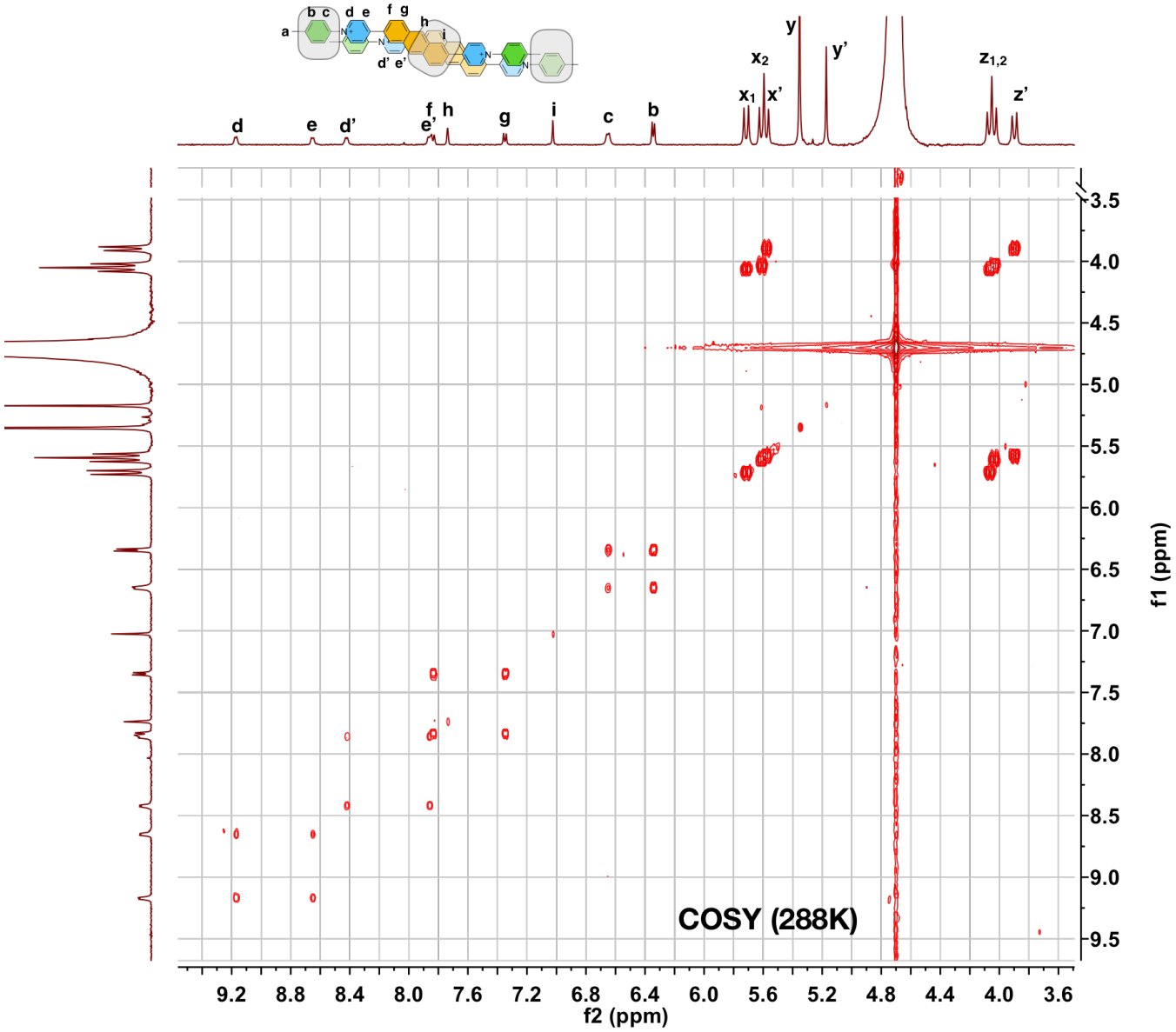

Figure S3. ^{1}H-^{1}H COSY spectra of **Ant26Me$_2$**-CB[8]$_3$ D_2O solution (65 μM) at 288 K.

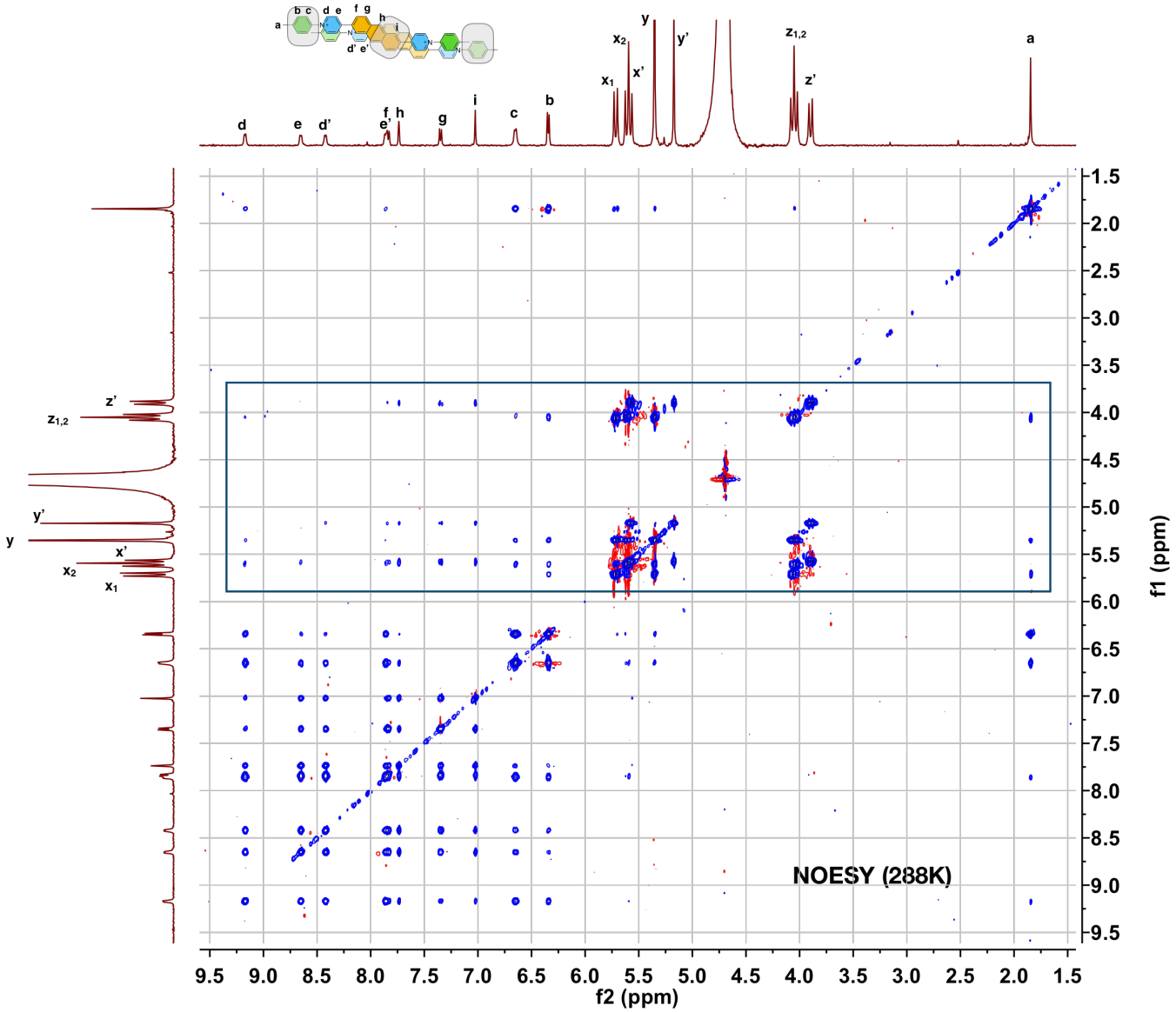

Figure S4. NOESY spectra of **Ant26Me$_2$**-CB[8]$_3$ D_2O solution (65 μM) at 288 K.

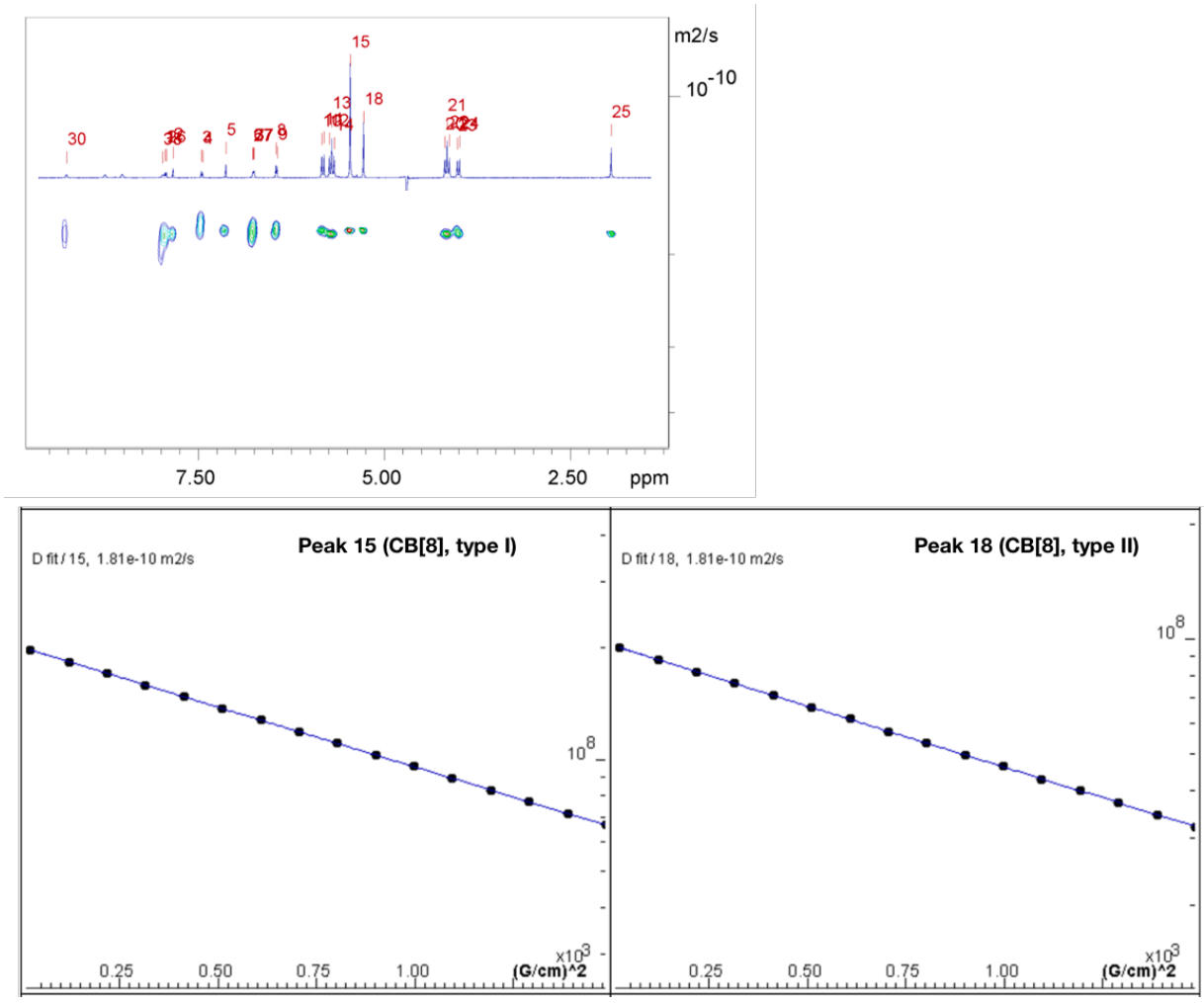

Figure S5. DOSY analysis of **Ant26Me$_2$**-CB[8]$_3$ D_2O solution (65 μM) at 298 K, showing one complex containing two type of CB[8] macrocycles with the same diffusion coefficient of 1.81x10^{-10} m^2/s.

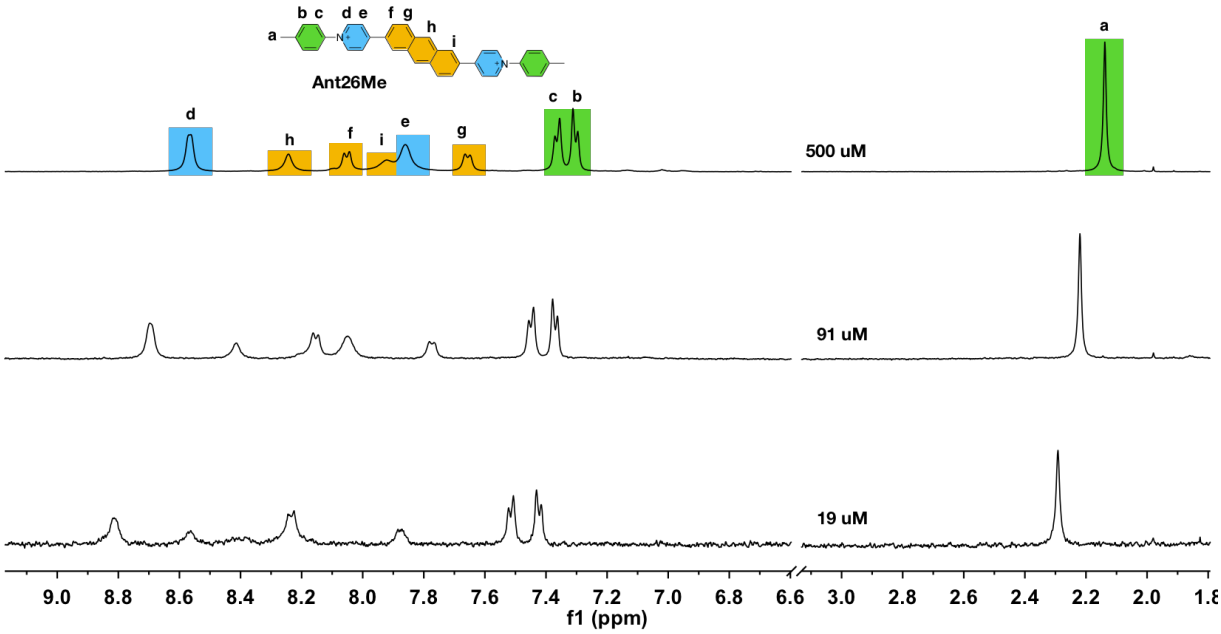

Figure S6. Concentration dependent of NMR spectra of **Ant26Me** D_2O solution at 298 K.

SI-4 Complexation of Np26Me with CB[7] and CB[8]

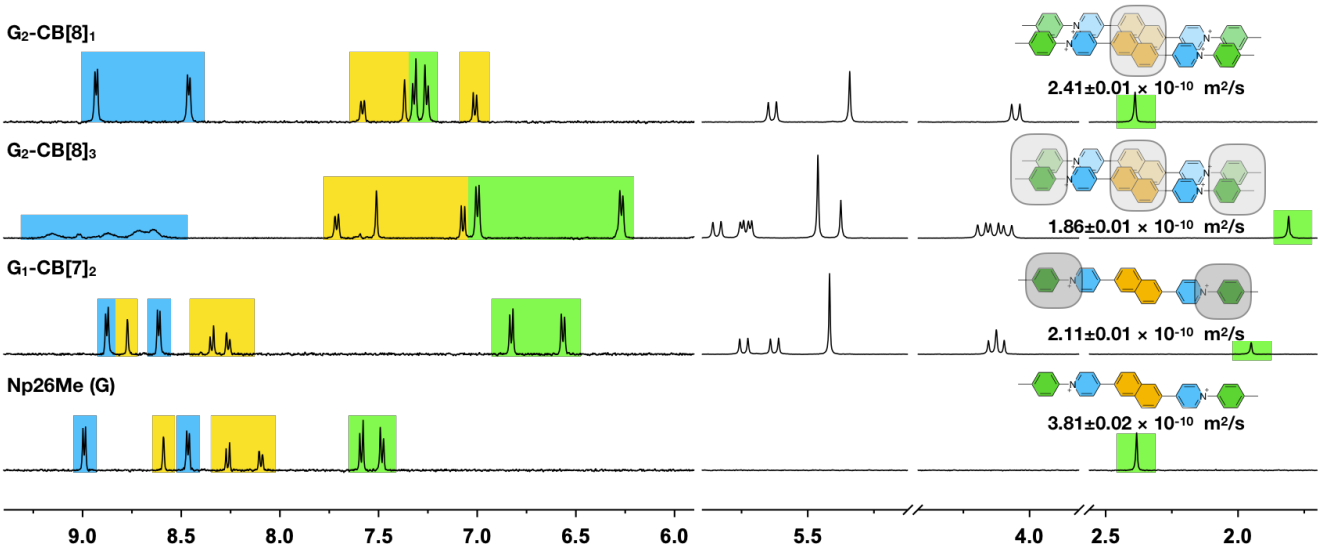

Figure S7. ^{1}H NMR spectra of **Np26Me** (G), G_1-CB[7]$_2$, G_2-CB[8]$_3$, and G_2-CB[8]$_1$ complexes in D_2O at 298 K. The broaden signals in G_2-CB[8]$_3$ between 8.5 and 9.5 ppm are pyridinium protons that experience a dynamic of intermediate rate related to NMR timescale. A detail study of this behavior will be presented in another work that is under review.

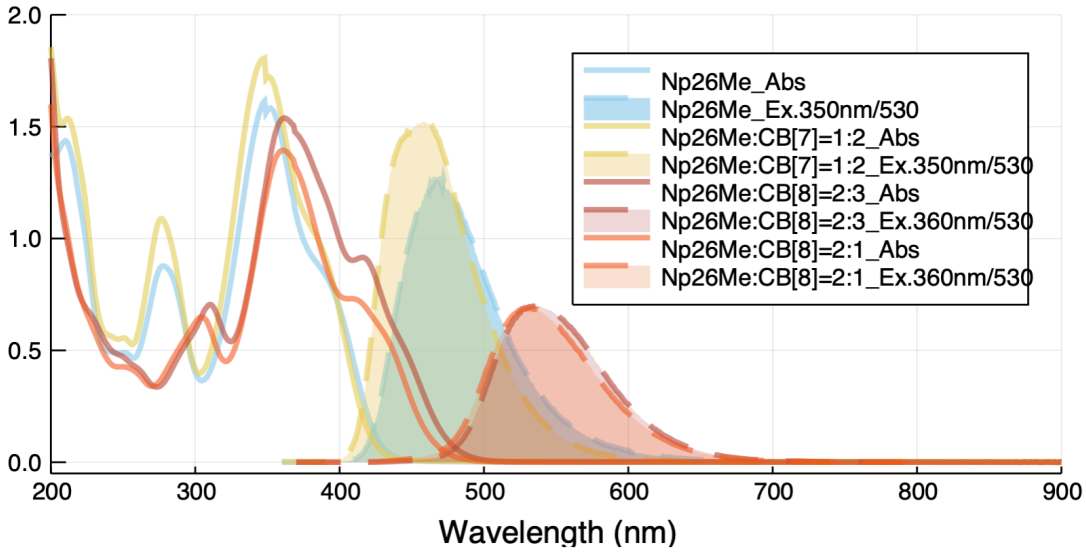

Figure S8. Absorption and emission spectra of **Np26Me** (G), G_1-CB[7]$_2$, G_2-CB[8]$_3$, and G_2-CB[8]$_1$ complexes in D_2O at 298 K with the same [G] of 30 μM. The profile of G_2-CB[8]$_3$ (red) and G_2-CB[8]$_1$ (orange) are almost the same.

SI-5 Chemical shift analysis of Np14R$_1$-CB[7]$_2$ complexes

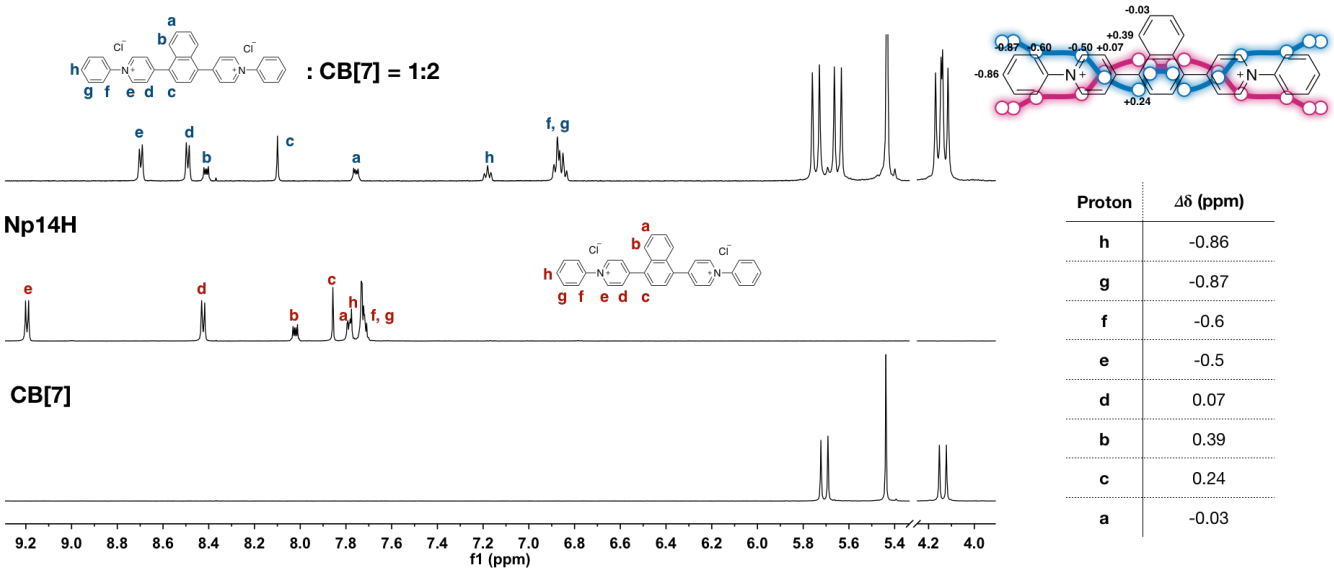

Proton	Δδ (ppm)
h	-0.86
g	-0.87
f	-0.6
e	-0.5
d	0.07
b	0.39
c	0.24
a	-0.03

Figure S9. The change of chemical shift (***Δδ***) of **Np14H** before and after complexation with CB[7] in D_2O at 298 K. The blue and red porfiles represent the chemical shift change of protons above and below the long-molecular axis, respectively, after complexation with CB[7].

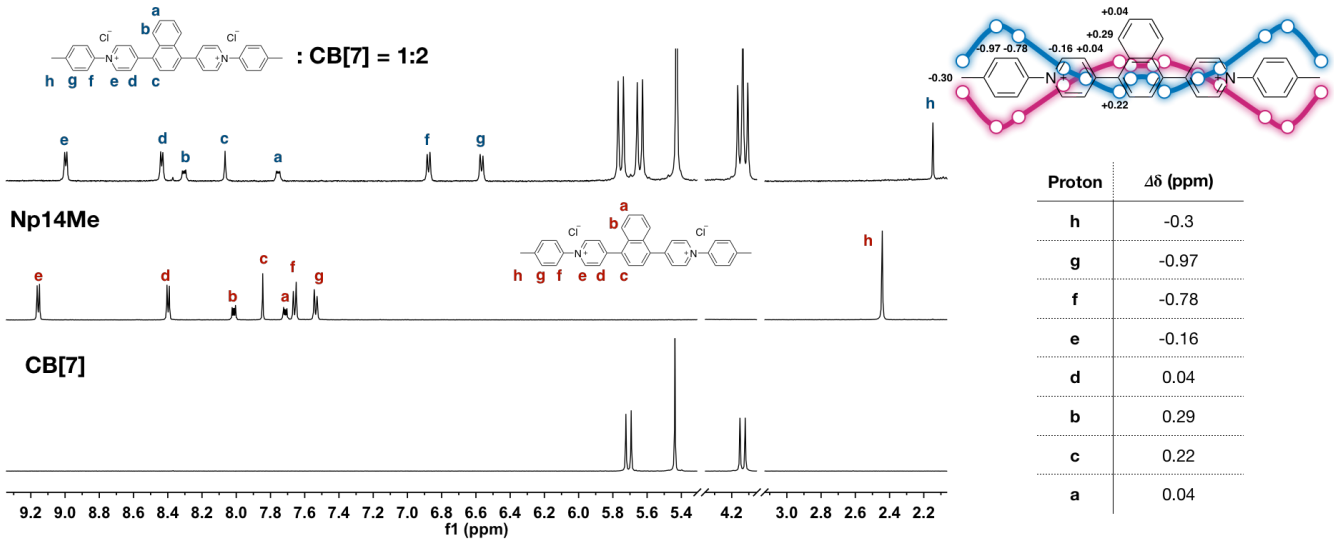

Proton	Δδ (ppm)
h	-0.3
g	-0.97
f	-0.78
e	-0.16
d	0.04
b	0.29
c	0.22
a	0.04

Figure S10. The change of chemical shift (***Δδ***) of **Np14Me** before and after complexation with CB[7] in D_2O at 298 K. The blue and red porfiles represent the chemical shift change of protons above and below the long-molecular axis, respectively, after complexation with CB[7].

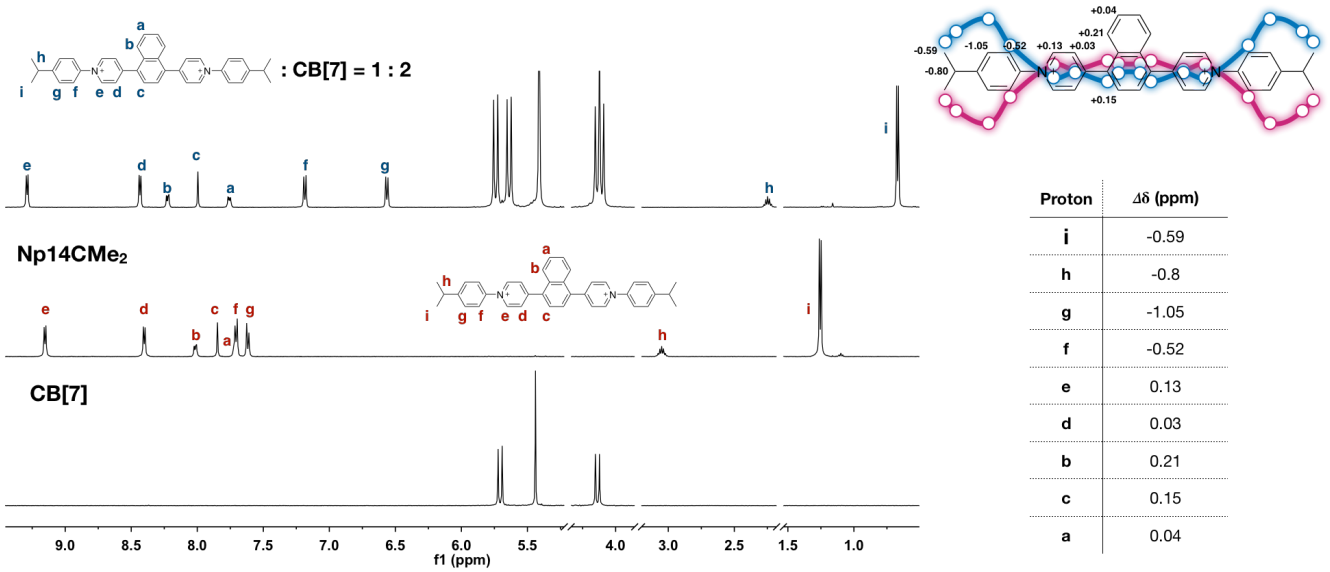

Proton	Δδ (ppm)
i	-0.59
h	-0.8
g	-1.05
f	-0.52
e	0.13
d	0.03
b	0.21
c	0.15
a	0.04

Figure S11. The change of chemical shift (*Δδ*) of **Np14CMe$_2$** before and after complexation with CB[7] in D_2O at 298 K. The blue and red porfiles represent the chemical shift change of protons above and below the long-molecular axis, respectively, after complexation with CB[7].

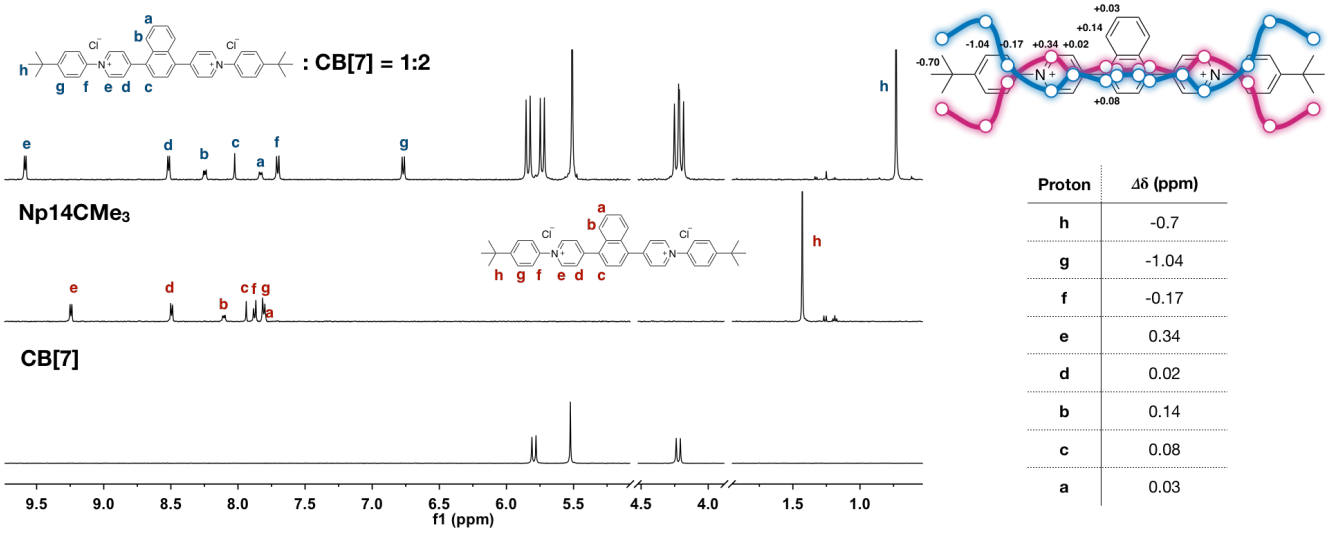

Proton	Δδ (ppm)
h	-0.7
g	-1.04
f	-0.17
e	0.34
d	0.02
b	0.14
c	0.08
a	0.03

Figure S12. The change of chemical shift (*Δδ*) of **Np14CMe$_3$** before and after complexation with CB[7] in D_2O at 298 K. The blue and red porfiles represent the chemical shift change of protons above and below the long-molecular axis, respectively, after complexation with CB[7].

SI-6 Complexation of Ph14CMe$_3$ with CB[8]

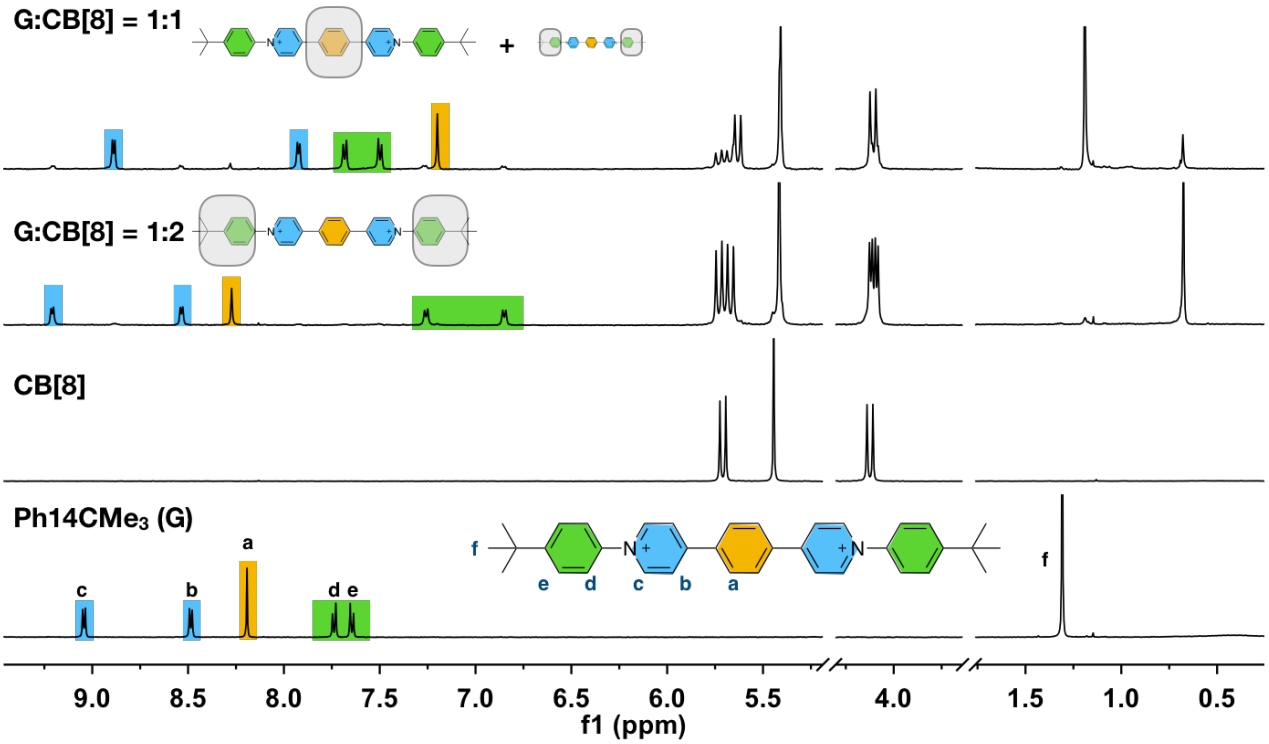

Figure S13. ^{1}H NMR spectra of **Ph14CMe$_3$** (G) and its mixture with 2 or 1 equiv. CB[8] in D_2O at 298K.

SI-7 Complexation of Ph14CMe$_2$ with CB[7] and CB[8]

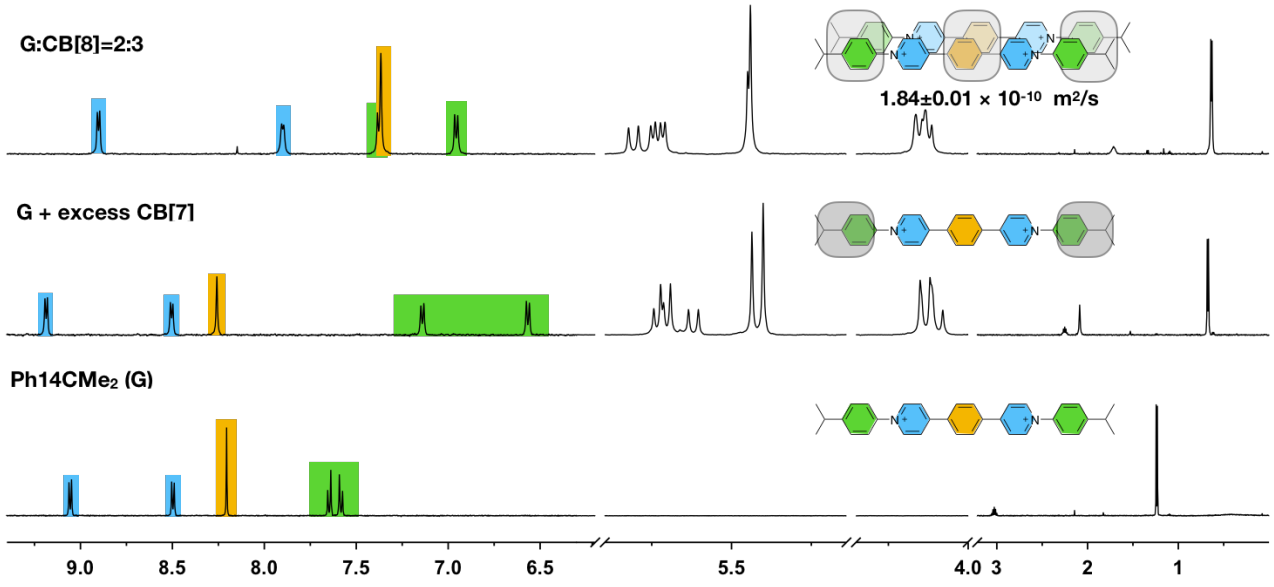

Figure S14. ^{1}H NMR spectra of **Ph14CMe$_2$** (G), G$_2$-CB[8]$_3$, and its complexation with excess CB[7] in D_2O at 298 K.

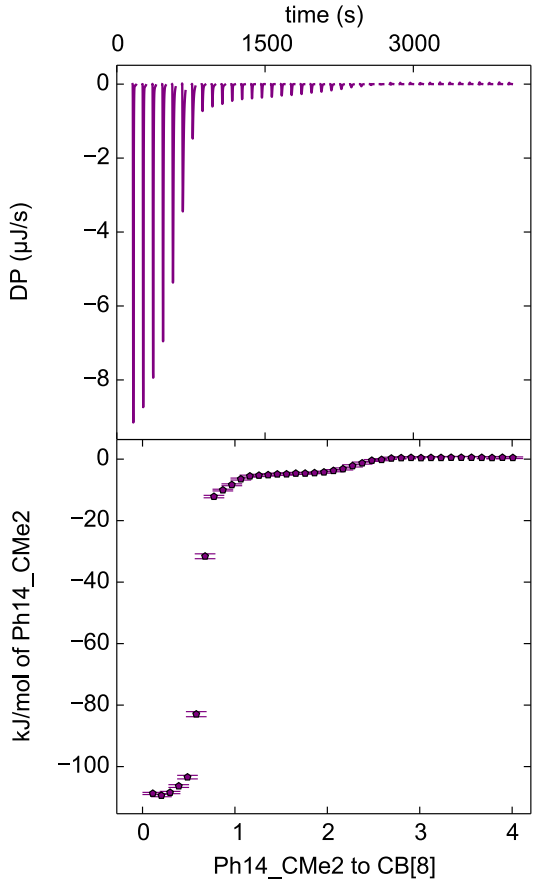

Figure S15. Titration of **Ph14CMe$_2$** (205 µM) into CB[8] (29.4 µM) in 10 mM sodium phosphate buffer (pH = 7) at 298 K, monitored by ITC, showing a first turning point at a G:CB[8] ratio of around 0.67 corresponding to the formation of G_2-CB[8]$_3$ complex.

SI-8 MD simulation

Molecular dynamics (MD) simulations were performed with the NAMD 2.12[6] program using the Amber generalized force-field.[7] the atomic charges were computed at the HF/6-31G(d) level of theory with the RESP scheme.[8] The **Ant910Me**$_2$-CB[8]$_2$, **Ant910Me**$_1$-CB[7]$_2$, MV$_1$-CB[8]$_1$, and MV$_1$-CB[7]$_1$ complexes were solvated in a TIP3P cubic water box with 4000 H_2O molecules using the Packmol software package.[9] The system was neutralized by adding Cl^- ions to the system.

Our MD protocol consisted of the following steps: (1) energy minimization over 10000 steps using a timestep of 1 fs; (2) equilibration over 2 ns in the NVT ensemble (T = 298.15 K) with the RMSD of heavy atoms in CB[n] (n = 7 and 8), **Ant910Me** and **MV** constrained to their initial position using a force constant of 1 kcal·mol^{-1}·Å^{-2}; (3) 4 ns equilibration run in the NPT ensemble (p = 1.01325 bar, T = 298.15 K); (4) 600 ns free simulation in the NPT ensemble, where the temperature and pressure were held constant at 298.15 K and 1.0 atm, respectively; (5) 200 ns production run to obtain the free energy profiles under the same conditions as (4). Constant temperature was set by a Langevin thermostat with a collision frequency of 1 ps^{-1}, whereas the target pressure was reached using the Berendsen barostat with the relaxation time set to 2 ps. All of the bonds and angles involving hydrogen atoms were constrained by the SHAKE[10] algorithm. We used the particle mesh Ewald method[11] for the long-range electrostatics in combination with a 12 Å cutoff for the evaluation of the non-bonded interactions. The equations of motion were integrated with a time step equal to 2 fs.

At step (4) of the MD protocol no bias was imposed on the intermolecular motions to probe the stability of the host-guest complexes. None of the complexes dissociated within the timescale considered.
The free energy profiles at step (5) were obtained with the Adaptive Biasing Force (ABF) method[12,13] as implemented in the NAMD 2.12 program, which is based on the thermodynamic integration of the free energy gradient. The free energy is expressed in terms of the reaction coordinate (z) defined as the projection of the distance between the center-of-mass (COM) of CB[n] (n = 7 and 8) and COM of MV$_1$ or COM of the binding motif for **Ant910Me** onto the axis perpendicular to the CB[n] portals. The z collective variable was sampled in the (−4.75, 2.75) and (−4.75, 4.75) intervals for the **Ant910Me** $_2$-CB[n]$_2$ and MV$_1$-CB[n]$_1$ (n = 7 and 8) complexes, respectively, with the bin width δz set to 0.1 Å. A force constant of 100 kcal·mol^{-1}·Å^{-2} was used at the reaction coordinate boundaries. A minimum sampling of 1000 simulation steps at each bin was used to estimate the average force before the application of the ABF. The simulation of each system was performed until the convergence of the free energy profiles.

Reference

[1] Day, A.; Arnold, A. P.; Blanch, R. J.; Snushall, B. *J. Org. Chem.* **2001**, *66*, 8094–8100.

[2] Brautigam, C. A.; Zhao, H.; Vargas, C.; Keller, S.; Schuck, P. *Nat. Protocols* **2016**, *11*, 882–894.

[3] Ronson, T. K.; Meng, W.; Nitschke, J. R. *J. Am. Chem. Soc.* **2017**, *139,* 9698–9707.

[4] Bongard, D.; Möller, M.; Rao, S. N.; Corr, D.; Walder, L. *Helv. Chim. Acta* **2005,** *88,* 3200–3209.

[5] Olesińska, M.; Wu, G.; Gómez-Coca, S.; Antón-García, D.; Szabó, I.; Rosta, E.; Scherman, O. A. *Chem. Sci.* **2019**, DOI: 10.1039/C9SC03057C

[6] Phillips, J. C.; Braun, R.; Wang, W.; Gumbart, J.; Tajkhorshid, E.; Villa, E.; Chipot, C.; Skeel, R. D.; Kalé, L.; Schulten, K. *J. Comput. Chem.* **2005**, *26*, 1781–1802.

[7] D.A. Case, I.Y. Ben-Shalom, S.R. Brozell, D.S. Cerutti, T.E. Cheatham, III, V.W.D. Cruzeiro, T.A. Darden, R.E. Duke, D. Ghoreishi, M.K. Gilson, H. Gohlke, A.W. Goetz, D. Greene, R Harris, N. Homeyer, S. Izadi, A. Kovalenko, T. Kurtzman, T.S. Lee, S. LeGrand, P. Li, C. Lin, J. Liu, T. Luchko, R. Luo, D.J. Mermelstein, K.M. Merz, Y. Miao, G. Monard, C. Nguyen, H. Nguyen, I. Omelyan, A. Onufriev, F. Pan, R. Qi, D.R. Roe, A. Roitberg, C. Sagui, S. Schott-Verdugo, J. Shen, C.L. Simmerling, J. Smith, R. Salomon-Ferrer, J. Swails, R.C. Walker, J. Wang, H. Wei, R.M. Wolf, X. Wu, L. Xiao, D.M. York and P.A. Kollman (2018), AMBER 2018, University of California, San Francisco.

[8] Wang, J.; Cieplak, P.; Kollman P. A. *J. Comput. Chem*. **2000**, *21*, 1049-1074.

[9] Martínez, L.; Andrade, R.; Birgin, E. G.; Martínez, J. M. *J. Comput. Chem.* **2009**, *30*, 2157–2164.

[10] Andersen, H. C. *J. Comput. Phys.* **1983**, *52*, 24–34.

[11] Darden, T.; York, D.; Pedersen, L. *J. Chem. Phys.* **1993**, *98*, 10089–10092.

[12] Darve, E.; Rodríguez-Gómez, D.; Pohorille, A. *J. Chem. Phys.* **2008**, *128*, 144120–144133.

[13] Hénin, J.; Fiorin, G.; Chipot, C.; Klein, M. L. *J. Chem. Theory Comput.* **2010**, *6*, 35–47.